

Supporting Information

Toettcher et al. 10.1073/pnas.0806196106

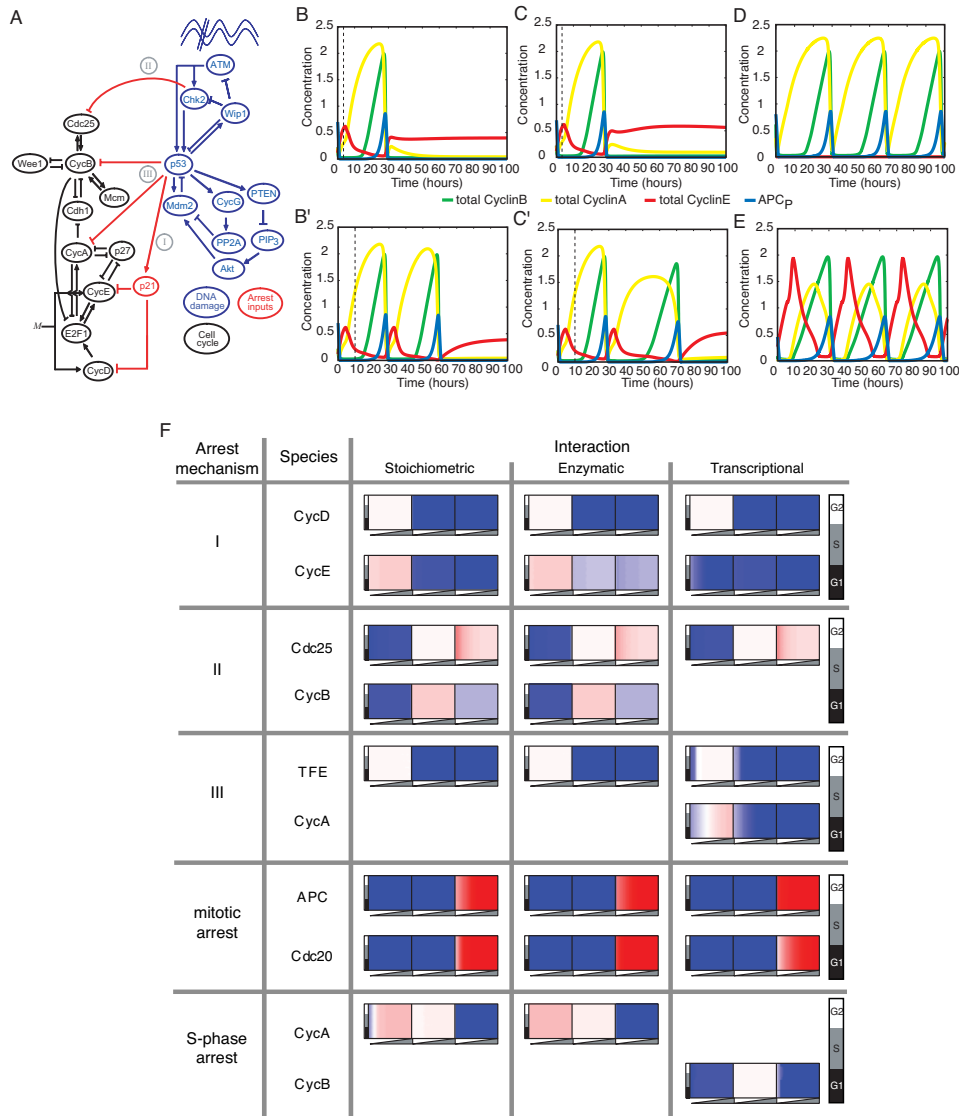


Fig. S1. Construction of a combined cell cycle and DNA damage model. (A) Diagram of the cell cycle and DNA damage models. Arrest mechanisms are labeled in gray. Mechanism I indicates the p53-dependent G1 arrest induced by p21. Mechanism II indicates Cdc25 phosphorylation and inactivation by Chk2 and its subsequent inhibition by 14-3-3 proteins. Mechanism III models the p53-dependent transcriptional repression of cyclin B and cyclin A. Additional feedback loops involving p53 are shown but do not significantly affect the network's dynamics in their current parameterization. (B–E) Matching experiments from the literature. Trajectories from the initial model are plotted for all simulations, showing levels of total cyclins B, A, and E and phosphorylated APC (APC_p) over 100 h. (B) Serum starvation applied 3 h (dotted line) after cell division leads to immediate G1 arrest. (B') Serum starvation applied 10 h (dotted line) after cell division leads to a G1 arrest after the completion of 1 full cell division. (C and C') Cycloheximide treatment applied 3 and 10 h after cell division have phenotypes similar to those achieved by serum starvation. (D) The cyclin E^{-/-} model, simulated with a mitogen level $M = 2$, is able to cycle. (E) Similarly, the cyclin D^{-/-} model cycles with $M = 10$. (F) Systematic inhibition of each cell cycle protein. Each group of 3 boxes is colored as described for Fig. 2. Inhibition of each cell cycle protein is applied by binding, enzymatic modification, or transcriptional repression by an inhibitor. The resulting arrest states are grouped into similar mechanisms: (i) mechanism I-like arrests result in a G1 DNA content state with high levels of G1 cyclins and low levels of G2 cyclins; (ii) mechanism II-like G2 arrests lead to a high G2 cyclin and low G1 cyclin state; (iii) mechanism III-like G2 arrests result in a high G1 cyclin and low G2 cyclin state; (iv) the model can also arrest in a mitotic arrest state by inhibition of APC or Cdc20, in which high active cyclin B levels maintain a mitotic state; and (v) an S-phase arrest state consisting of high cyclin A levels but low cyclin B levels can arise from cyclin B repression or cyclin A inhibition.

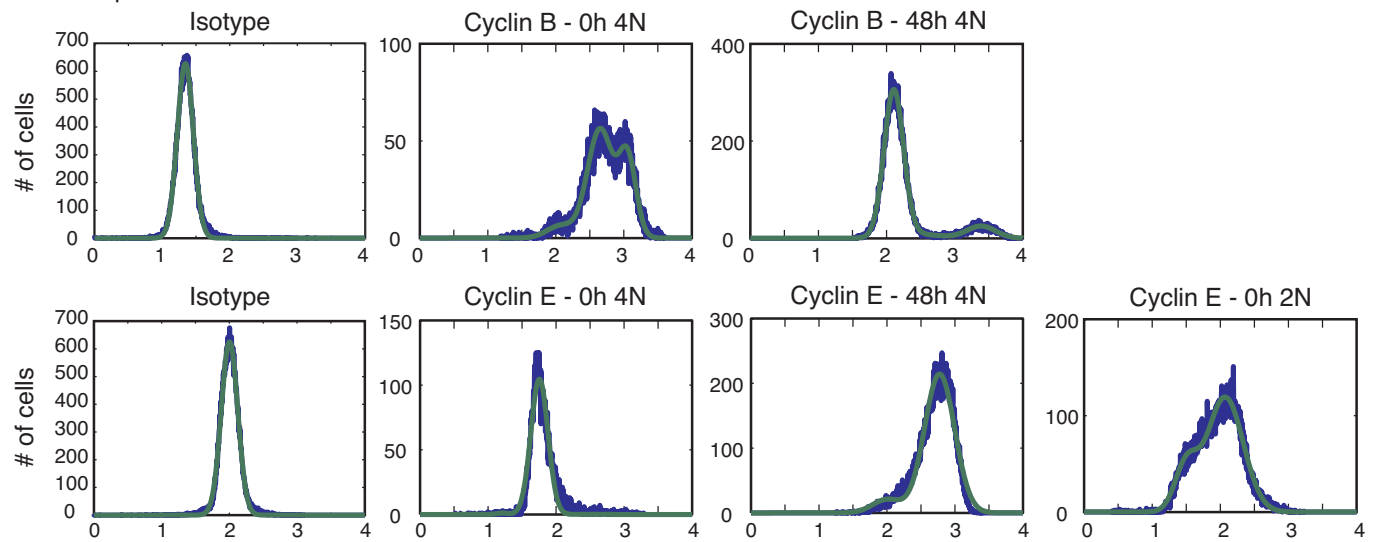
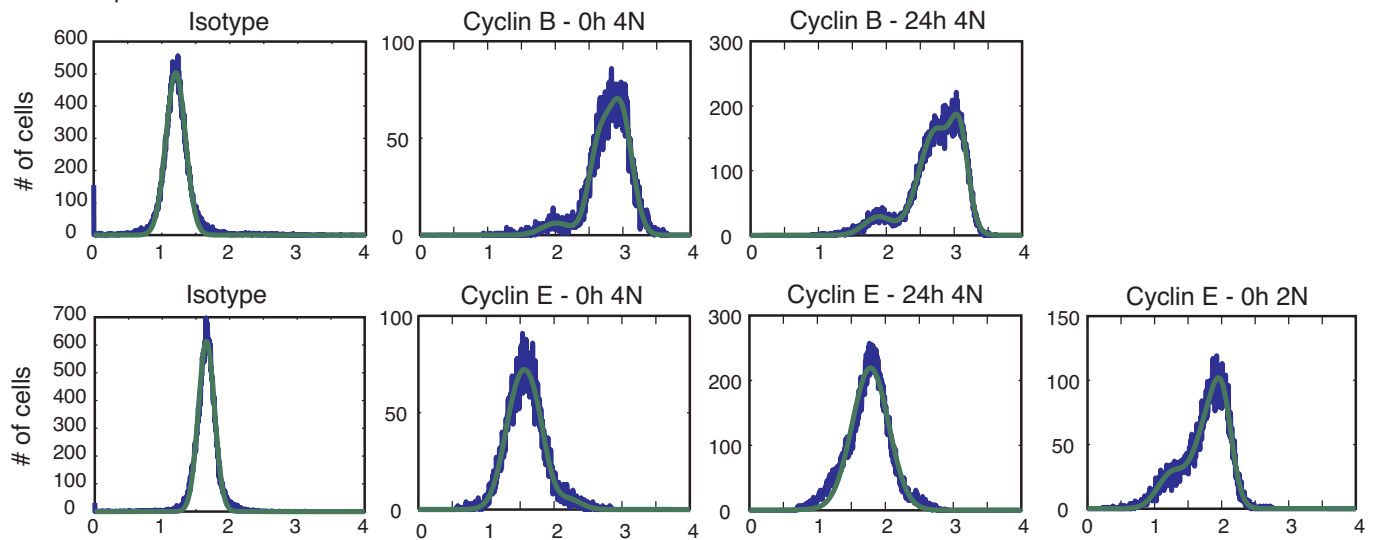
A HCT p53^{+/+}B HCT p53^{-/-}

Fig. S3. Log-normal fits for isotype control and cyclin levels. (A) Distribution of cyclin B and E levels in HCT p53^{+/+} cells. Cyclin B levels in cells with 4N DNA content showed 3 peaks, probably representing G2 cells (intermediate), mitotic cells (high), and cells after metaphase but before cytokinesis (low). The sum of 3 Gaussian distributions (green) was fitted to the measured data (blue). Cyclin E levels in cells with 4N DNA content were unimodal. In cells with 2N DNA content, they were bimodal, probably representing early (low) and late G1 cells (high). The measured distributions were fitted with single Gaussian and the sum of 2 Gaussian distributions, respectively. The distribution of the respective isotype controls were fitted with single Gaussian distributions. (B) Distributions of cyclin B and cyclin E levels in HCT p53^{-/-} cells. The measured data were fitted as described above.

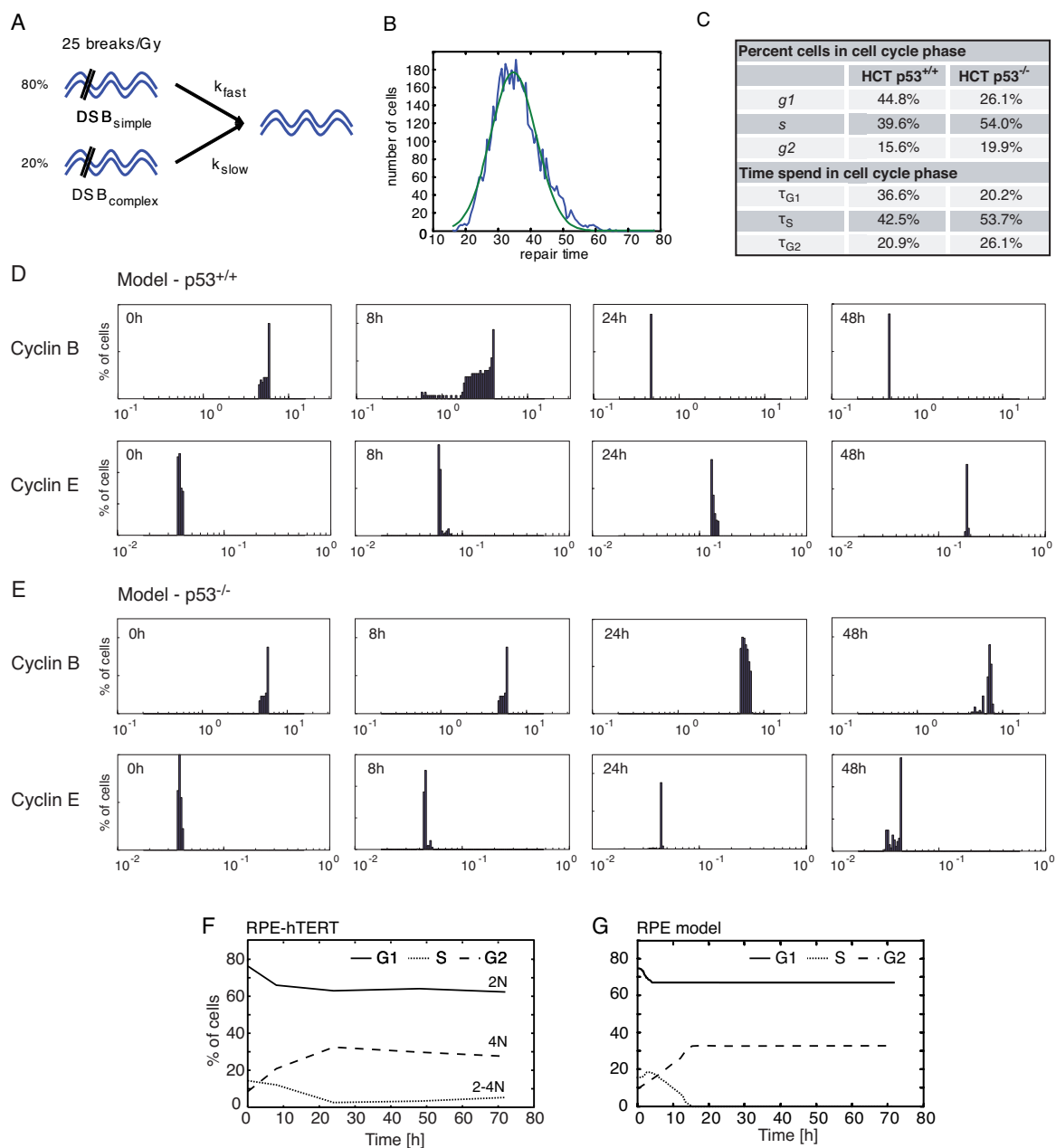


Fig. S4. Simulating populations of cells after DNA damage. (A) Diagram of the stochastic DNA double-stranded break (DSB) repair model. See *SI Appendix* for details. (B) Distribution of repair times from the model (blue curve), compared with a normal distribution with mean 35 h and SD 10 h (green curve). Two types of DSBs—easy and difficult to repair—were modeled, with an initial distribution of 80% and 20% of the total damage, respectively. Easy breaks were repaired with a half-life of 15 min, whereas difficult breaks were repaired with a half-life of 10 h. The initial number of breaks was distributed according to a Poisson distribution with a mean of 25 DSBs/Gy IR, and repair was assumed to occur when fewer than 3 breaks remained. (C) The difference between the fraction of cells in G₁, S, and G₂ and the mean time spent by each cell in these phases. Results for both wild-type and p53^{-/-} cells are shown. The rows labeled *g*₁, *s*, and *g*₂ indicate the fractions of cells in each cell cycle phase as determined by flow cytometry analysis. The rows labeled τ_{G1} , τ_S , and τ_{G2} indicate the mean time spent in each cell cycle phase, as computed from Eq. 9. (D and E) Cyclin distributions from fitted models. The same ensemble of models used to generate the population data of Fig. 4 C and D was queried for cyclin levels during arrest. (D) Histograms of total cyclin B and E levels are shown at 0, 8, 24, and 48 h after IR for the p53^{+/+} model. The log species concentration is plotted as the independent variable. Cyclin B levels decrease quickly, whereas cyclin E levels rise gradually by 48 h. (E) Corresponding histograms of total cyclin B and E levels in the p53^{-/-} model. Levels of both species are largely maintained during arrest, with an increase in variability as cells re-enter the cell cycle. (F) Time courses of DNA content after treatment with 10 Gy IR. RPE-hTERT cells were irradiated at 0 h, and the fractions of cells with G₁, S, and G₂ DNA contents were measured by FACS. The same graph is shown in Fig. S2. (G) Model-generated cell cycle distribution time courses. The model was adjusted to fit the different cell cycle times of RPE-hTERT cells. Individual model trajectories (500) were simulated from initial conditions distributed through the cell cycle (see *SI Appendix*). In each simulation, p53 was induced 4 h after damage was applied. The DNA repair time was selected from the distribution described in B (see *SI Appendix*).

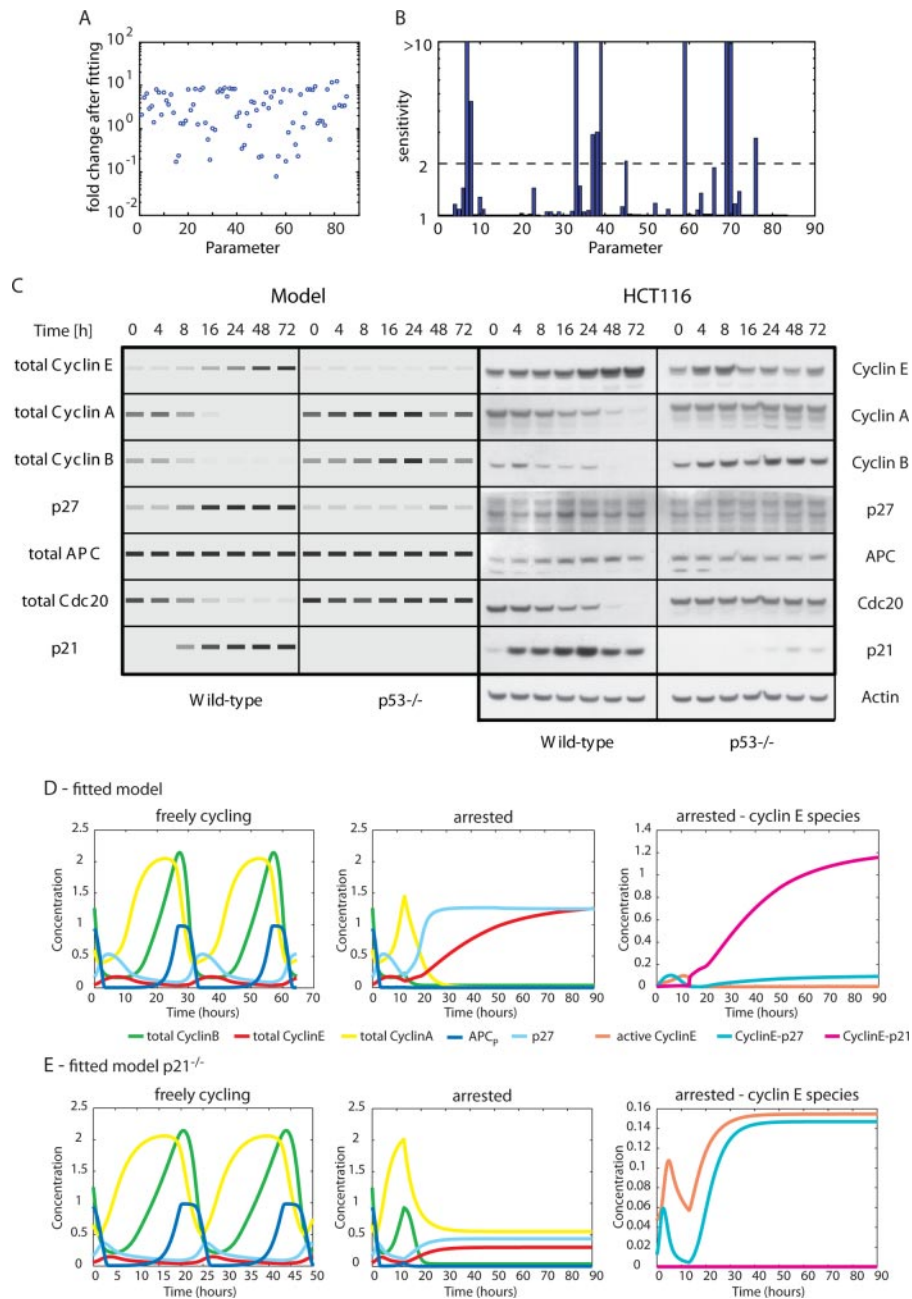


Fig. S5. Validation of the fitted model. (A) Influence of optimization on parameters. The index number of each fitted parameter in the cell cycle arrest model is plotted against the fold change in that parameter between the initial and final parameterization. To compute this change in parameterization, both initial and final parameter sets were scaled such that the period of the p53^{+/+} model was 30 h. (B) Parameters constrained by optimization to the objective function. The plot indicates the fold change in parameter value required to increase the objective function value by 0.1 for each parameter considered in optimizing the cell cycle arrest model. Bars corresponding to parameters that vary more than a 10-fold are cut off at this value. The horizontal dotted line indicates a 2-fold parameter change. Parameters that are unconstrained to more than a 2-fold change are listed in Table S3. (C) Predicted protein levels in fitted p53^{+/+} and p53^{-/-} models. Total concentrations of cyclins A, E, and B, p27, APC, Cdc20, and p21 were measured from a simulated population of 500 cells after induction of damage. Intensity varies linearly with the concentration of each species, and both cell lines are plotted on the same scale. The same species' total protein levels were measured in HCT p53^{+/+} and p53^{-/-} cells by Western blot. [Antibodies: APC2 (M. Kirschner), p27 (Santa Cruz Biotechnology; catalog no. 1641), and Cdc20/p55cdc (Santa Cruz Biotechnology; catalog no. 1906).] (D) Cell cycle simulation from the fitted model showing cyclins E, A, and B and phosphorylated APC (APC_p). In the absence of DNA damage, the fitted model shows qualitatively similar behavior as the initial model, with consecutive peaks of cyclin E, cyclin A, cyclin B, and APC_p. When DNA damage is applied during G2 phase (13 h), the model arrests with low levels of cyclins A and B and high levels of total cyclin E. The level of active cyclin E is low, because it is bound by p21 (and to a lesser extent by p27). (E) Cell cycle simulation in the absence of p21. Without damage, the p21^{-/-} model behaves similarly to the full model. When DNA damage is applied during G2 phase (13 h), the model arrests with low cyclin B levels but intermediate cyclin A levels. Cyclin E levels are higher than in freely cycling cells but lower than during arrest in the full model. In contrast to the full model, cyclin E is active and reaches levels higher than during the normal G1/S peak, because inhibition by p27 alone is insufficient. Therefore, cells are predicted to enter S phase without going through mitosis (which would be indicated by a pulse of APC_p), leading to endoreduplication.

Other Supporting Information Files

[Table S1 \(PDF\)](#)

[Table S2 \(PDF\)](#)

[Table S3 \(PDF\)](#)

[Table S4 \(PDF\)](#)

[SI Appendix](#)

[MATLAB code](#)